High Speed Optical Imaging Photon Counting Microchannel Plate Detectors for Astronomical and Space Sensing Applications

Oswald Siegmund, John Vallerga, Barry Welsh, Jason McPhate, Anton Tremsin,
Space Sciences Laboratory, U.C. Berkeley

ABSTRACT

Cross delay line and cross strip high resolution position encoding readouts have the capability of being able to independently record the accurate time of each detected photon event without compromising the imaging performance. This is important for time dependent UV-Visible applications in ground based and space astronomy, biology, night-time reconnaissance and time of flight instruments. We have developed sealed tube microchannel plate cross strip (18 mm) and cross delay line (25 mm) anode detectors with visible light photocathodes. These have high spatial resolution, are capable of high counting rates and provide extended lifetimes. High-speed electronics for the cross strip readout have been developed and accommodate > 5 MHz random photon rates, and we have demonstrated time tagging of events with ~1ns accuracy. Spatial resolutions of < 30 μm with excellent image linearity have been achieved in tests of an 18 mm cross strip anode sealed tube detector. The 25 mm cross delay line sealed tube has been commissioned on the South African Large Telescope 10m telescope and performed a variety of high time resolution observations of transient and time-variable astronomical sources.

Keywords: Microchannel plate, photon counting, imaging, timing

1. INTRODUCTION

In recent years we have implemented a variety of high-resolution, photon-counting Microchannel plate (MCP) detectors in space instrumentation for satellite (FUSE [1], GALEX [2], IMAGE [3], SOHO [4], HST-COS [5]), rocket, and shuttle payloads as well as sensors for ground based astronomy, reconnaissance and biology. These detectors satisfy the imaging and timing demands of applications including astronomy of transient and time-variable sources [6], Earth atmospheric imaging and spectroscopy for real time space weather monitoring, biological single-molecule fluorescence lifetime imaging microscopy [7], airborne and space situational awareness, and optical night-time reconnaissance [8]. Our recent work on high performance photon counting imaging readouts has enabled significant advancements over previous detector systems used for these applications.

We have developed Cross-Strip (XS) and Cross-Delay-Line (XDL) event position encoding anodes, and have integrated them into detector systems with readout electronics. Sealed tube MCP detectors with formats of 18mm (XS) (Fig. 1) and 25mm (XDL) (Fig. 2), with visible light sensitive photocathodes have been built and are currently being used for biological fluorescence lifetime imaging microscopy [9], and ground based high time resolution astronomy [6] respectively. Using the XS sealed tube detector and a new generation of event encoding electronics we can achieve high spatial resolution (< 30 μm FWHM) with self triggered ~1 ns event timing accuracy at up to ~10 MHz event rates.

Our installation and astronomical commissioning of one of these detectors at the South African Astronomical Observatory (SAAO), South African Large Telescope (SALT) 10m telescope has enabled us to observe a number of transient and time-variable sources. Our photometer is positioned in an auxiliary instrument port of the SALT. This is a stand-alone instrument that includes our detector system with two filter wheels (neutral density and U, B, V), an iris, and all the control modules necessary to operate the system. This instrument gives us access to the southern sky with significant sensitivity and unprecedented time resolution (microsecond). High time resolution astronomy is still in its infancy, such that high cadence observations of the variable visible wavelength emission from cataclysmic variables, short period pulsars, M-dwarf flares, low mass X-ray binaries, flickering from black-holes in AGN, stellar occultations of solar system planets and high precision timing of transiting extra-solar planets are all topics of potential interest to the astronomical community. During two weeks of initial observations a large range of these objects were observed, including high time resolution observations of cataclysmic variables, pulsars, and flare stars.

2. SEALED TUBE DETECTOR SYSTEMS

2.1 Cross Delay Line Anode Detectors

The cross delay line (XDL) anode is a relatively coarse (~1 mm period) multi-layer metal and ceramic pattern on an alumina substrate (Fig. 3). On one surface of the substrate a conductor is fabricated as a serpentine approximately 0.5 mm wide. Then sets of insulating and conducting fingers are applied in the orthogonal direction such that 50 % of the

bottom layer is left exposed, while keeping the crosstalk between axes negligible. The top and bottom serpentine conductors are used to collect the charge from the MCPs with equal charge sharing between the axes. XDL anodes are low outgassing, accommodate >800°C temperatures, and are compatible with sealed tube high vacuum devices. Position readout is achieved by measuring the difference in the time of arrival of the signals at the two ends of the delay line serpentine for each axis. Encoding electronics is well established (amplifier/time to digital conversion) and can accommodate good spatial (<25µm [5, 11, 12]) and timing resolution (~100ps [7, 9, 10]).

Fig. 1. 25 mm cross delay line anode, MCP, sealed tube with S20 photocathode.

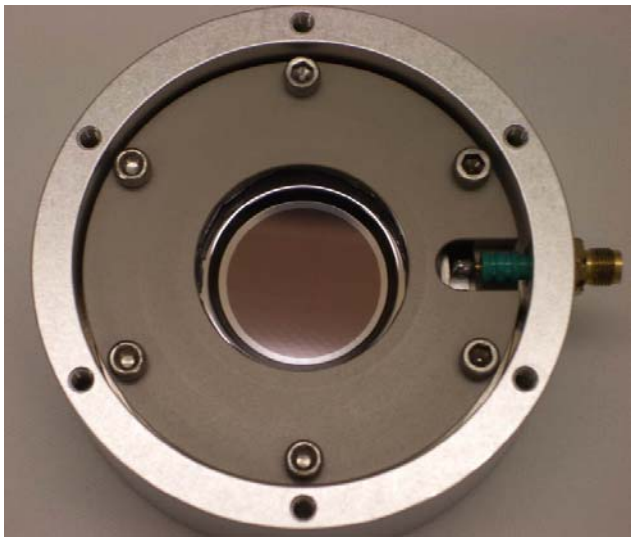

Fig. 2. 18 mm cross strip anode, MCP, sealed tube with SuperGenII photocathode, assembled into housing.

Cross delay line detectors have been used for a number of applications including biological fluorescence lifetime imaging [9], synchrotron excited photoelectron emission spectroscopy [10], time resolved astronomical observations from ground [6], space based instruments [11], and neutron imaging [13]. We have fabricated a sealed tube 25mm cross delay line MCP sealed tube detector (Fig. 1) with an S20 photocathode for our instrument that is being used at the SALT 10m telescope. The peak QE of this tube is less than 10% (at 400nm), and the cathode has no extended red response. However the background is low (few 10s of events/sec) and no cooling is required. The electronics allows us to achieve >1 MHz event rates and event time stamping of the order 20ns, which is sufficient for many uses on SALT. New sealed tubes with higher QE are currently being made to replace this initial "pathfinder" detector.

2.2 Cross Strip Anode Detectors

The improvements in spatial resolution, counting rate and lifetime are most important for many potential future applications. To achieve these enhancements we have been developing the cross strip anode (Fig. 4). Rather than a continuous serpentine anode pattern in each of the axes, the XS anode is comprised of an array of isolated strips, or "fingers" for each axis. The MCP charge cloud is matched to the anode period (~0.6 mm) so that charge is collected on several neighboring fingers to ensure an accurate event centroid can be determined [14]. XS anodes are mounted ~3 mm behind the MCPs and each strip is connected through a hermetically sealed hole to the backside of the anode, allowing mounting of all the detector electronics outside the vacuum enclosure. Only two MCPs are needed since the electron gain required is less than 10^6.We have previously reported results with a 32 x 32 mm XS open face laboratory detector, demonstrating excellent resolution (<7 µm FWHM) using low MCP gain (~5 x 10^5) [14]. More recently [15] detectors with anodes up to 50mm x 50mm format, and smaller 22mm formats (Fig. 4) have been made. The 22mm XS anodes are currently being used in both open face and sealed tube MCP detectors for UV, and visible light. We have recently completed an 18mm sealed tube detector using the 22mm XS anode (Fig 2) and a pair of 6µm pore MCPs. Tests with this device and our newest Parallel Cross Strip (PXS) electronics show significant performance enhancements compared with the XDL sealed tubes and earlier XS detector electronics. Specifically the SuperGenII photocathode (Fig. 5) that was deposited by Photonis during tube fabrication has higher QE and redder response than our S20 photocathode tubes. It is currently being commissioned for an application in biological fluorescence lifetime microscopy [9].

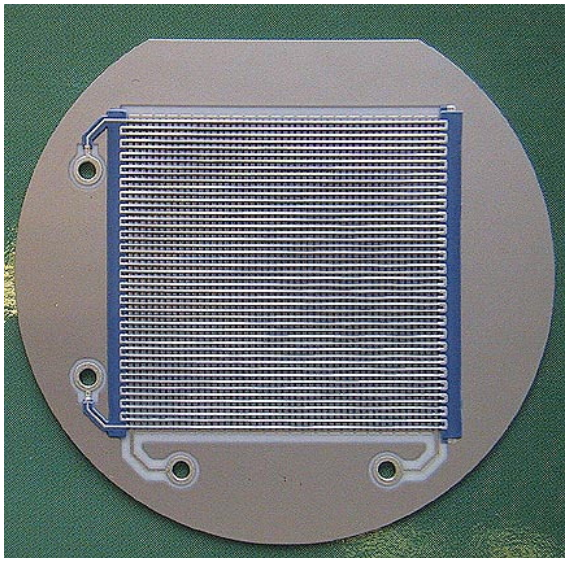

Fig. 3. 29 mm cross delay line anode with plated through contact holes for the delay line signals.

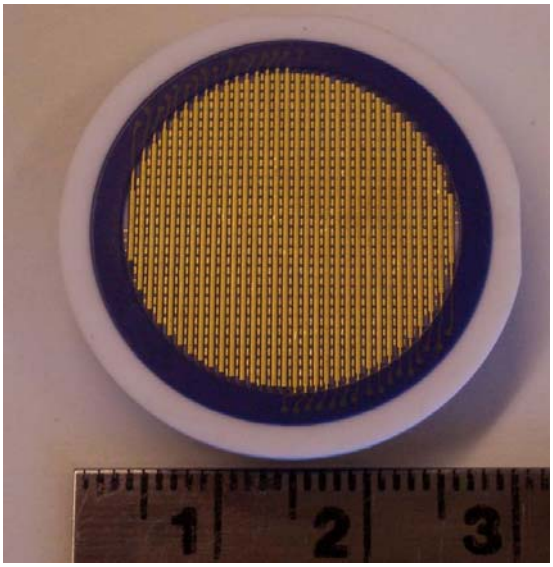

Fig. 4. 22mm XS anode with 32 x 32 strips and buried contact vias through the substrate to the anode backside.

2.3 Cross Strip Event Encoding Electronics

To derive event positions, each finger of an XS anode is connected to a charge sensitive amplifier. This is followed by subsequent analog to digital conversion of individual strip charge values, and calculation of event centroids. This is accomplished by software, or firmware, algorithms which also account for amplifier gain variations, linearity, pulse shape and offsets. The recently developed high speed parallel electronics (PXS) [15] digitizes the strip signals, and processes the events to generate the X, Y position with a resolution of <20 µm and time stamps the events with sub-nanosecond accuracy. In the parallel encoding scheme each strip on the anode is connected directly to a preamp input of a 2 x 32 channel ASIC (RD-20) amplifier board [15]. The output of these preamplifiers are shaped unipolar pulses with ~40 ns rise time, ~160 ns fall time with a measured noise of ~1000 e^- RMS. The parallel signals (2 RD-20's per board) are buffer-amplified before being sent via a coaxial ribbon cable to be continuously digitized by 64 (8 octal packs) analog to digital converters operating at 50 mega-samples per second. These digital samples are transferred to an FPGA (Xilinx Virtex 5) using a LVDS serial stream where they are digitally filtered to extract event pulse peak information [15]. A FIR, or custom, filter is used to determine the peak charge on the neighboring strips affected by an incident event, and corrections are applied to the data to account for amplifier gain variations, gain non-linearities, offsets and pedestals. The results are then used to derive the event centroid for both X and Y axes. This centroid position is combined with a timing tag. A coarse time tag (< 20ns) is obtained using the FPGA clock counter. Interpolation of the digitized pulse, using a pulse shape model, can then be used to derive timing accuracy to the order of 1ns. All the events are buffered and transferred to a downstream PC as an event list of X, Y and T for storage, and/or binning and display. The configuration of the electronics depends on the detector format used. The 22mm XS anode (Fig. 4) as implemented in the 18mm sealed tube (Fig. 2) requires only one RD20 board (2 x 32 channels) and one PXS system. In the case of the 40 mm XS detector [15] two RD20 amplifier boards and two PXS systems (one for X and one for Y) are required.

2.4 Cross Strip Detector Tests

The 18mm XS tube with a SuperGenII photocathode (Figs. 1, 5) is being used for applications in biology [9], future tubes will be used for night-time remote sensing and ground based astronomy [6]. Ultimately we plan to employ GaAs photocathodes to replace the SuperGenII photocathodes giving increased efficiency and acceptable dark noise (< 100 events/sec) provided cooling (-10°C) is used.

Our initial tests with the combined R20/PXS system and the 22 mm XS tube have benefited from considerable effort in optimization of the system by implementing algorithms in FPGA firmware. The performance with respect to fixed pattern noise, spatial and timing resolution, and event rate handling limits are not necessarily satisfied by the same optimizations. Our standard test strategy is to project a resolution test mask image with small pinholes at regular intervals onto the photocathode to assess spatial resolution and image linearity. A result for the 18 mm XS tube is shown in Figs. 6, and 7, which demonstrates good image linearity. The spatial resolution for this test was measured as ~30µm FWHM, which deteriorates somewhat as the event rate is increased to ~8 MHz input rate due to event pile-up. The rate was progressively increased by increasing the diffuse flux and leaving the projected pinhole images constant.

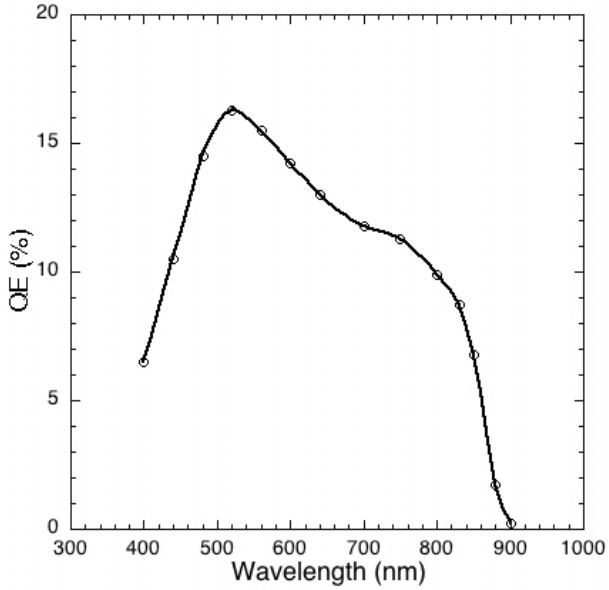

Fig. 5. Photocathode quantum efficiency for the 18 mm cross strip anode sealed tube detector (SuperGenII).

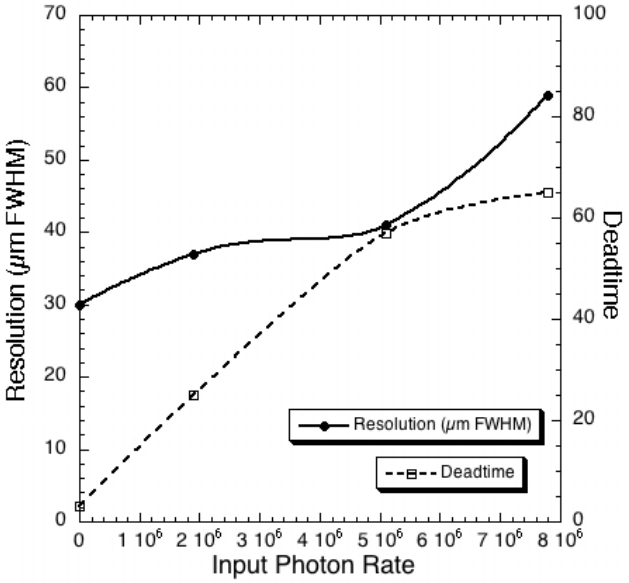

Fig. 6. Spatial resolution and electronics dead time % as a function of input event rate, 18mm XS tube.

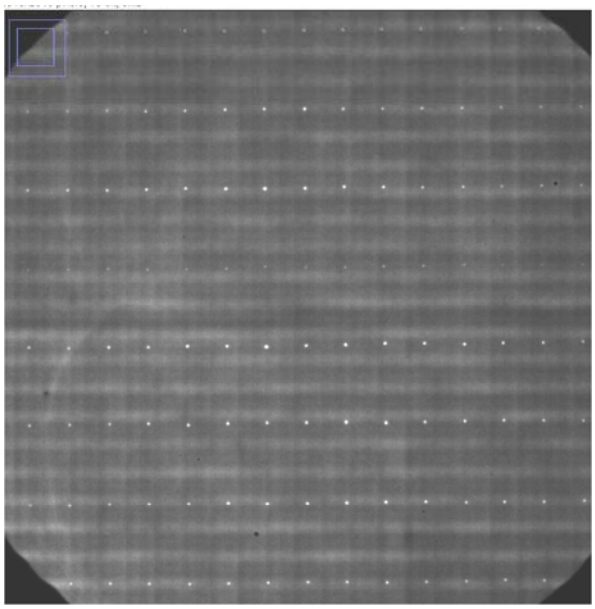

Fig. 7. Image of a 2 mm x 1mm spaced 25μm spot array with a 2 MHz diffuse background. 18 mm XS tube / PXS.

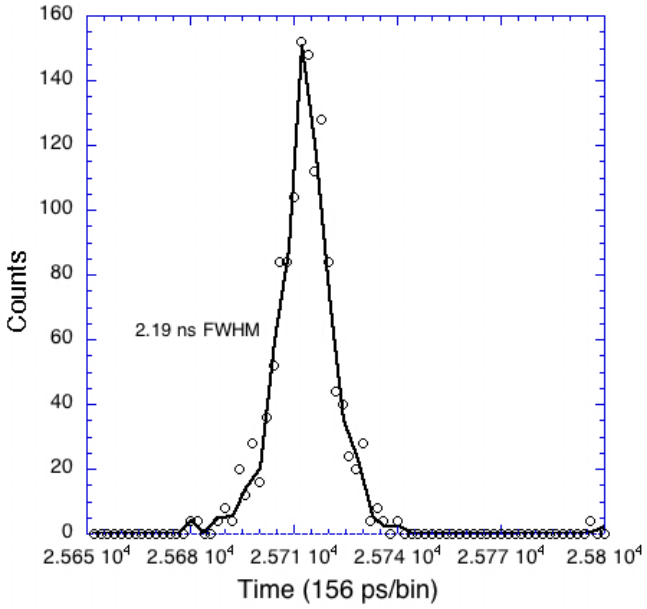

Fig. 8. Measured 18 mm XS tube time jitter for laser pulse time intervals using the PXS electronics system.

The current PXS system firmware/software using our standard centroiding algorithms assume a single event at a time on the detector. So to avoid excessive event pile-up due to the decay time of the amplifier, we applied an event time window to allow baseline restoration. This has the effect of increasing the system dead time (Fig. 6) but limits the degradation of resolution. We are currently investigating faster amplifiers and pulse shaping techniques to allow more rapid baseline restoration and hence higher counting rates with less effect on the resolution. The resolution achieved at low rates is dominated by the sealed tube proximity gap and the projected input point spread function. The image in Fig. 7 does show some residual fixed pattern noise (banding, ~5%), which is due to the finger structure. This can be almost completely removed with better firmware algorithms, but these have not been fully optimized yet.

Using laser pulse inputs, the timing resolution for successive laser pulse events has also been investigated. We have used interpolation of the FPGA clock timing using FIR filtering of the input signals. In this way we can achieve

~2 ns time tag jitter (Fig. 8) on the events. This contrasts with <1ns for electronics stimulation pulses. Current work in progress is aimed at optimization of the FPGA firmware code to achieve the best performance for all the detector tests.

3. OBSERVATIONS WITH THE SAAO SALT 10M TELESCOPE

3.1 Berkeley Visible Image Tube (BVIT) on SALT

The BVIT system developed for (and presently mounted on) the SALT telescope is an improved version of the previous prototype photon counting detector system used at the Lick Observatory in 2006-2007 [6] and is a self-contained enclosed unit that is mounted near to the prime focus of the SALT 10m mirror system (Fig. 9). In this position it has a 1.9 arc min field of view, thus enabling easy source acquisition and associated recognition, with the added ability to simultaneously monitor comparison stars present in the field-of-view and also the sky background signal throughout the observational period. In Fig. 10 we show the system as installed into the auxiliary bay at SALT in early 2009. Light from the SALT multi-mirror system enters the BVIT enclosure through an adjustable field of view iris. The incident beam then passes through a filter wheel with user-selectable Johnson U,B,V and ND filters and ultimately focuses onto the BVIT detector window. Photon events are converted into electrons and gain multiplied to produce charge signals on the cross delay-line readout anode which are then amplified and subsequently digitized for data processing using a Xilinx based FPGA ADC board. Power to the detector and electronics units is provided by high and low voltage supplies mounted within the BVIT enclosure. The digitized photon signals are then sent via a data port to a high speed data processing unit capable of handling rates up to ~ 1.1 MHz. These data (in the form of photon X,Y positions and arrival times) are stored on a 0.5 Tera-byte hard disk mounted to a mini-ITX PC. Command and control of the BVIT high voltage, filter selection, shutter, iris aperture size, file handling and quick-look inspection is achieved via a ground support PC. The XDL detector that we have made at UCB (Section 2.1, Fig. 1) was used at SALT. However, we are in the process of making higher efficiency (SuperGen II photocathode) tubes at Photonis/DEP (Netherlands). Implementing these new sealed tubes with higher efficiency in combination with large SALT 10m telescope aperture will provide much higher sensitivity (x10) over a wider bandpass, but also higher event rates and higher background sky rates. We will also upgrade the computer and electronics to accommodate this when the new tube installation is done.

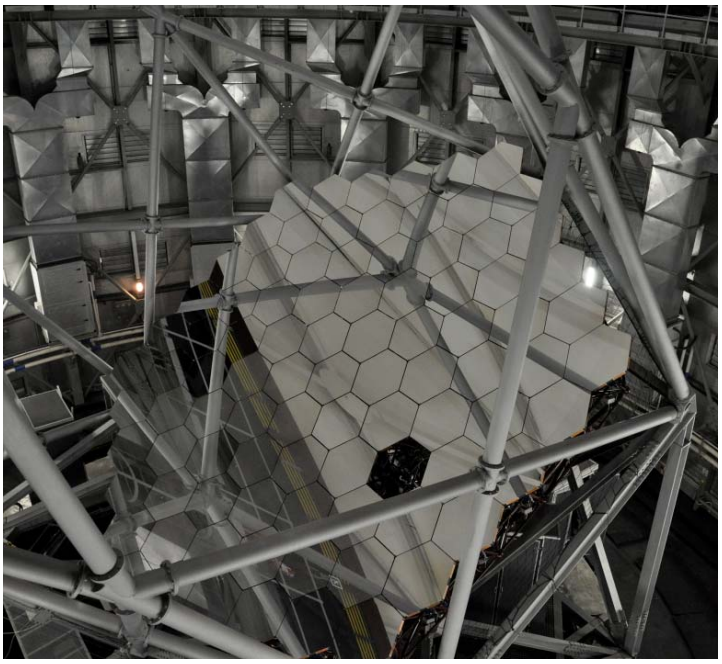

Fig.. 9. The SAAO SALT 10m telescope mirror

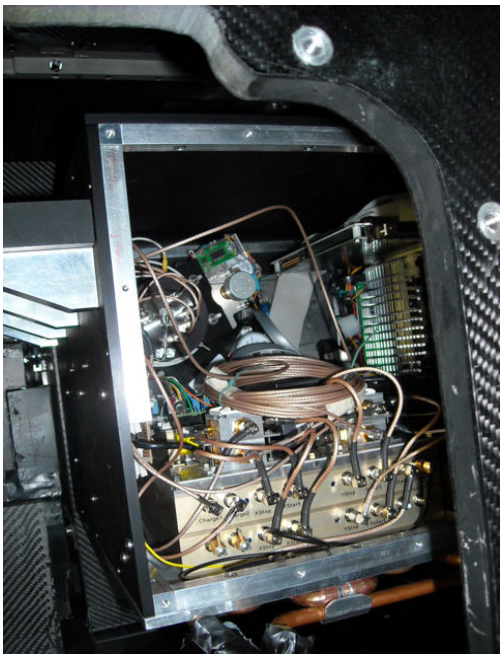

Fig.. 10. The BVIT camera system on SALT

3.2 Scientific observations

Observations were recorded with the BVIT on SALT during the two `engineering runs'. The data are currently being analyzed in a more rigorous scientific manner and we present the following as an indication as to the capability and type of observations that this instrumentation can presently achieve. Future observations using this system will also include stellar occultations by asteroids & Kuiper Belt Objects, in addition to observations of the Vela pulsar.

3.2.1 GX 339-4 (Black Hole candidate)

This black hole X-ray transient is a low mass X-ray binary that undergoes significant X-ray, optical and radio outbursts separated by years or even longer periods of quiescence. In its low X-ray state the source is typically associated with an optically bright counterpart, during which fast flickering on time-scales as short as 20ms has been previously observed [16]. In the high state, soft X-ray emission generated in the accretion disk dominates. A still unanswered question concerning this (and other) black hole candidates is the physical origin of the rapidly variable optical emission. Two likely candidate processes for this optical emission are optically thin synchrotron emission or non-thermal emission within a relativistic outflow or jet [17]. In Fig. 11 we show a typical 500sec long time series observation of GX 339-4 (shown in 1 sec time-bins) recorded on this $m_v \sim 16.0$ object with BVIT on SALT that shows several very fast eruptive events. In Fig. 12 we show an expanded profile (data in 0.1 sec bins) of a large event recorded during a later exposure that shows significant physical structure originating on time-scales of < 0.5 seconds. In order to progress further on identifying the possible origin of the optical emission we will require simultaneous real-time X-ray data (with the XTE satellite), since a testable prediction from the relativistic outflow model is that the strength of the positive CCF signal should be related to the prominence of the jet. As the source goes from low to a hard state we would expect the jet to increase in strength, as should the related optical fractional variability (rms) of the data.

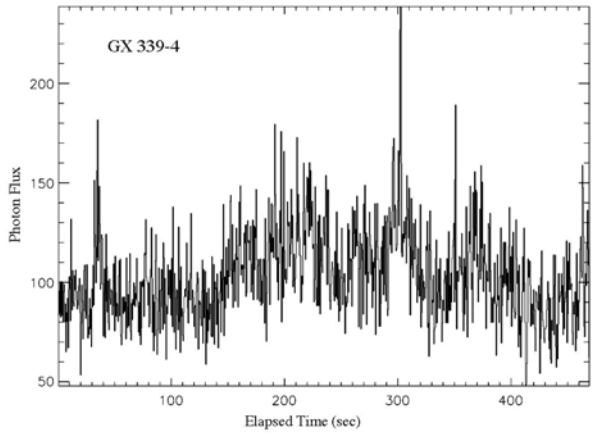

Fig. 11: *500s BVIT B-band observation of the black hole candidate GX 339-4 showing several fast eruptive events*

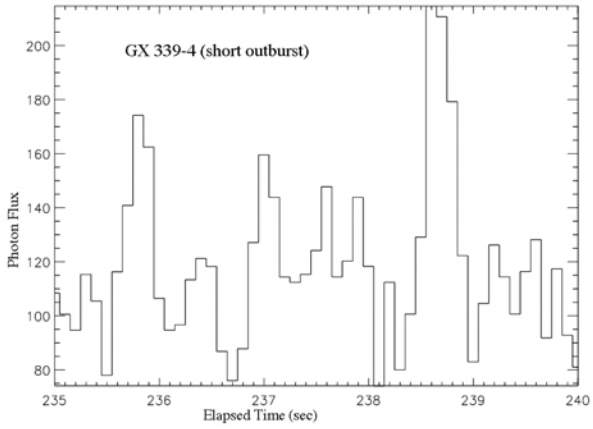

Fig. 12: *Eruptive event on GX 339-4 showing physical structure on time-scales < 0.5 sec*

We note that [18] found a 50% rms variability when the source was in a bright low/hard state, while [18] found only a 15% rms variability in the faint low/hard state. In Fig. 13 we show a power spectrum of a 600 sec BVIT observation of GX339-4 (with 0.03125s binning and the source in a low state) over-plotted with a simple power-law index of 0.85 +/-0.02 that indicates a fractional variability rms of ~16%, in agreement with the observations of [19].

3.2.2 UZ For (AM Her-type CV)

This 18th magnitude star is an AM Her binary (or polar cataclysmic variable) in which the strong magnetic field of the white dwarf primary causes it to rotate synchronously with the orbital motion. The magnetic field also prevents the formation of an accretion disc around the white dwarf. The accretion stream from the Roche lobe filling secondary M-type star is funneled along the magnetic field lines and impacts the white dwarf near a magnetic pole. The system has a 126.5-min orbital period, close to the lower edge of the 2–3 h 'period gap', a sparsely populated region in the orbital period distribution of cataclysmic variables. UZ For has also been observed to exhibit transient flare events in both the X-ray and optical/UV regimes [20]. The orbital eclipse has been studied previously with lower time resolution at visible wavelengths [21] and in Fig. 14 we show our present observations of a UZ For eclipse in time bins of 0.5s. Our new data shows that the eclipse lasts for ~ 469s and it resolves the previously known two `emission bumps' located approximately half-way through the ingress and egress of the eclipse. These two features are due to the manner in which the accretion spot on the white dwarf is eclipsed by the inclined orbit of the M-type star. Our BVIT data now allows the study of rapid aperiodic optical variability (i.e. flickering) associated with quasi-periodic oscillations (QPO's) on time-scales <0.5 sec. We have performed a Fourier spectral power analysis of these data, and although the data shows strong aperiodic variability (i.e. small flare-like flickering), the power spectrum showed no significant frequencies between 0.01 to10 Hz that could be associated with any potential QPO's.

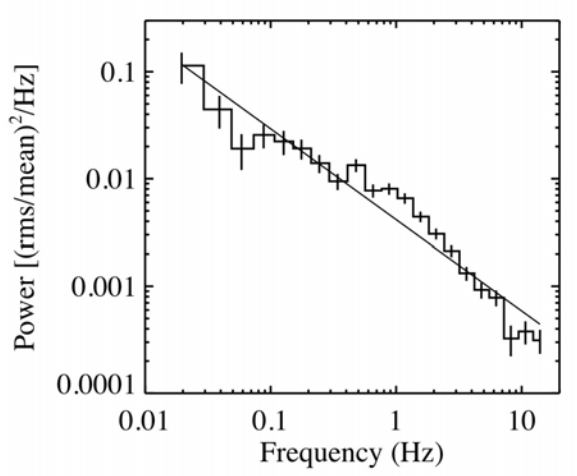

Fig. 13: *Power spectrum of the BVIT light curve from GX339-4*

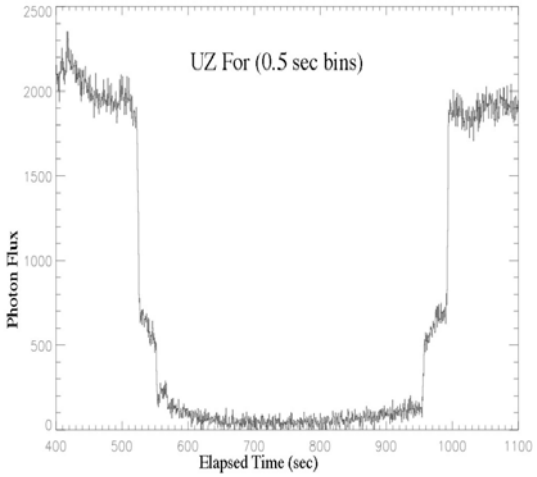

Fig. 14: *BVIT B-band eclipse of the UZ For system.*

The study of QPO's (at both X-ray and visible wavelengths) is important since [22] has identified a correlation between the high-frequency quasi-coherent oscillations of cataclysmic variables and the kilohertz QPOs of low mass X-ray binaries that extends over 2 orders of magnitude in frequency. This would suggest that the same physical mechanism that produce the QPOs operates in white dwarfs, neutron stars, and black hole binaries, and thus it should be related to disk accretion onto any low magnetic field compact object.

3.2.3 CN Leo (M5.5V flare star)

This is a well-known flare star which has recently been the focus of a multi-wavelength observing campaign during which a giant flare was observed [23]. We were fortunate to observe two smaller flares (only ~ 500 sec apart) during one of our BVIT observations on SALT, as shown in Fig. 15. The flare emission recorded in our pass-band (3600 – 5100Å) is predominantly due to a significant increase in the photospheric continuum level, superposed with many chromospheric emission lines.

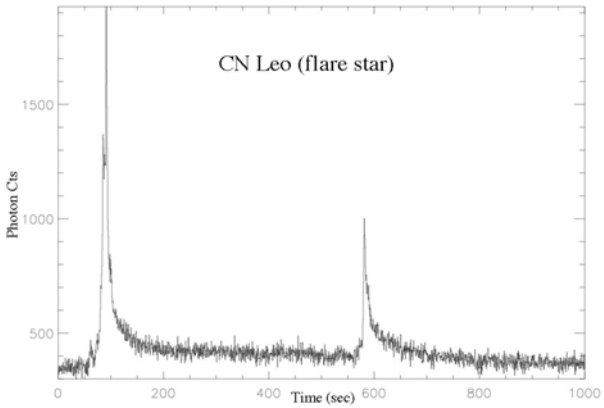

Fig. 15: *BVIT observations (1sec bins) of 2 flares on the star CN Leo*

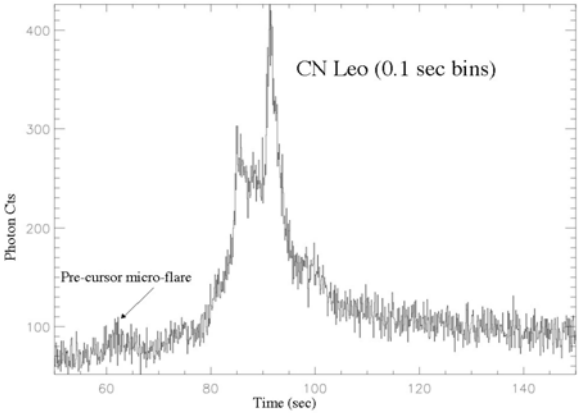

Fig. 16: *BVIT observations (0.1 sec bins) of time structure of micro-flares on CN Leo*

In Fig. 16 we show an expanded view of the first flare, in time bins of 0.1 s. Our observations clearly resolve two important aspects of the flare mechanism; (1) the detection of at least one small micro-flare (at t ~ 62 s) that is a pre-cursor to the main flare event (which itself could be considered to be composed of a giant micro-flare at t ~85 s followed by the main flare event at t ~90s), and (b) considerable structure in the flare emission itself on timescales < 0.1 s. Such observations (although unfortunately not accompanied by co-ordinated X-ray observations) are important since heating by microflares (and nanoflares) has been proposed to explain the heating of the corona of the Sun and that of other stars [24] This model assumes that any coronal loop is composed of many unresolved strands of magnetic flux and that these strands are heated impulsively by small bursts of energy called microflares. Such models specifically

assume an impulsive heating of the strands of magnetic flux, which can be recognized only in data with very high time resolution (i.e. < 1s).

3.2.4 V1033 Cen (AM Her-type CV)

This is a faint (m_v ~ 16.5) and little-studied AM Her cataclysmic variable system that BVIT observed in an unusually high state of activity. Previous X-ray observations were of insufficient duration to determine whether the associated emission originates from the accretion pole on the white dwarf [25], whereas visible photometric studies have revealed a period of ~3.16 h for the system with quasi-periodic oscillations being detected with time-scales in the 20 – 42min range [26]. The accretion region is appreciably extended in magnetic longitude and the associated emission observed at visible wavelengths is observed to be highly variable (see Fig. 17).

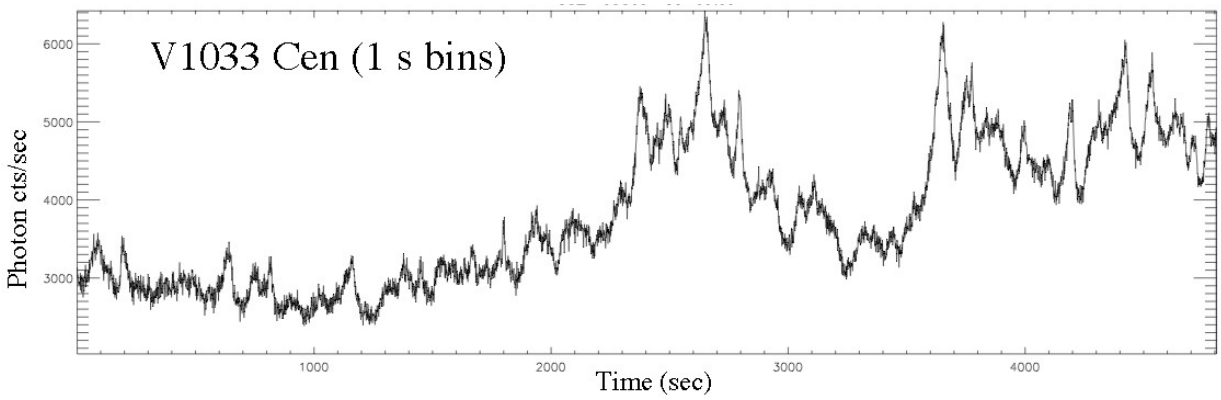

Fig. 17: *Highly variable emission from the AM Her CV system of V1033 Cen observed with the BVIT*

In Fig. 18 we show a FFT power analysis of this emission versus time signature that reveals weak evidence for quasi periodic oscillations for several periods in excess of 100s, in agreement with previous observations of this system by [26].

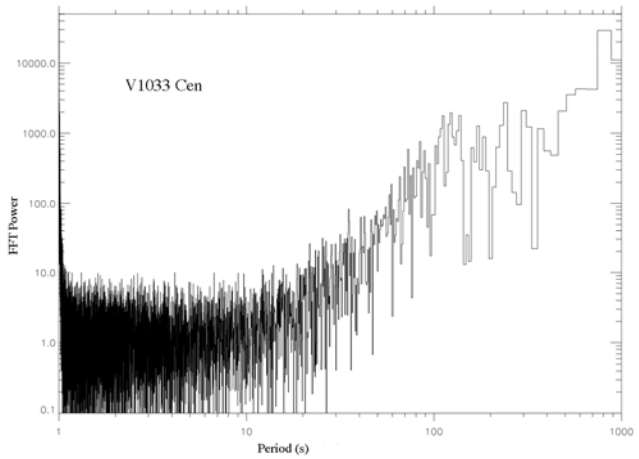

Fig. 18: *FFT power spectrum of emission from V1033 Cen*

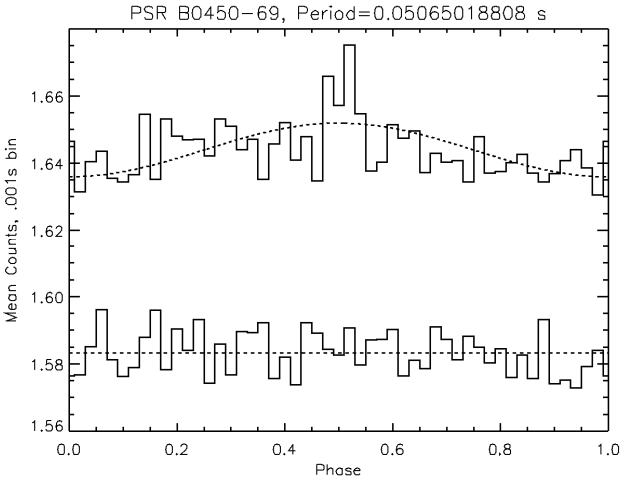

Fig. 19: *Phase of PSR B450-69 at the best-fit period of 0.05065s with a sinusoid pulse profile overplotted. Also shown - equivalent data for the background signal.*

3.2.5 PSR B0540-69 (pulsar)

This mili-second pulsar (located in the Large Magellanic Cloud) is usually referred as the 'Crab Twin' because of the similar period and period derivative with respect to the well-known Crab Pulsar. However, their pulse shapes are different: for the Crab it consists of two peaks, with a phase separation of about 0.4, that are visible at all wavelengths, while PSR B0540-69 has a single, broadly symmetric pulse about 0.5 wide in phase, with some structure at the maximum. Although hundreds of pulsars have been detected in the radio and X-ray regimes, because of their intrinsic optical faintness only 3 pulsars have had their pulse periods confirmed at visible wavelengths (i.e. the Crab and Vela pulsars and PSR B0540-69).

Our BVIT observations of PSR B0540-69 were aimed at (a) confirming the pulse period of ~ 50.4ms recorded at visible wavelengths, and (b) performing a search for intermittent `giant' fast optical pulses. These latter phenomena are sporadic, large-amplitude, short-duration (micro-second) bursts some 100 – 10,000 times more energetic than regular pulses that have recently reported from radio observations of several pulsars such as the Crab [27] and PSR J1820-30A [28]. These bursts are thought to be due to changes in the coherence of the radio emission and the pulse profiles are composed of many superposed nanosecond structures. Such tiny timescales imply tremendous brightness temperatures of ~ 10^{38} K making nanopulses the brightest pulses in the Universe, and thus challenge our understanding of pulsar magnetospheric physics. Visible observations of the Crab pulsar have shown that the optical pulses recorded during a giant radio pulse period are on average 3% brighter than normal optical pulses [29], but no `giant' optical pulses have yet been detected. The fact that the optical pulses are coincident with a giant radio pulse and also show slightly enhanced intensity suggests that the coherent (radio) and incoherent (optical) emissions produced in the Crab pulsar's magnetosphere are linked, and it has been argued that the optical emission is a reflection of the increased plasma density that causes the giant radio pulse event. Our 3000s BVIT observations of PSR B0540-69 have revealed no giant pulses (with a significance > 5-σ at the micro-second binning level) that could be similar in nature to those recorded at radio wavelengths. In addition, we have folded (or 'binned') the pulsar data at regular time intervals in order to determine the present pulsar period. In Fig. 19 we show our derived phase profile for a best-fit period of 50.65 ms, which is clearly only a marginal detection compared with the equivalent background signal. We note that [30] using a high efficiency wide-band GaAs photomultiplier required ~ 25,000 s on a 4m telescope to derive the pulsar period. Although our present observations have provided only a marginal measurement, we now have great confidence that with a new BVIT detector with an improvement in quantum efficiency of a factor of ~ 10, we shall be able to derive a pulsar period with high S/N ratio. Such an improved system will also enable a similar measurement on the slightly fainter Vela pulsar.

4. ACKNOWLEDGEMENTS

We acknowledge the efforts of R. Raffanti, Dr. X. Michalet, D. Rogers, J. Hull, J. Malloy, R. Barwhani, and Dr. D. Buckley, Dr. A. Gublis and the SALT team for their assistance in accomplishing these studies. This work was supported in part by NSF grants AST0352980 and DBI-0552-099, NASA grants NNX08AE04G and NNG05GC79G, and NIH grant NIBIB EB006353.

5. REFERENCES

1. O.H.W. Siegmund, M.A. Gummin, J.M. Stock, et. al, "Performance of the double delay line microchannel plate detect detectors for the Far-Ultraviolet-Spectroscopic Explorer", *Proc SPIE* 3114, pp.283-94, 1997.
2. O.H.W. Siegmund, P. Jelinsky, S. Jelinsky, et al., "High resolution cross delay line detectors for the GALEX mission", *Proc. SPIE* 3765, pp.429-40, 1999.
3. J.M. Stock, O.H.W. Siegmund, J.S. Hull, et al.,"Cross-delay-line microchannel plate detect detectors for the Spectrographic Imager on the IMAGE satellite", *Proc SPIE* 3445, pp.407-14, 1998.
4. O.H.W. Siegmund, M.A. Gummin, T. Sasseen, et al., "Microchannel plates for the UVCS and SUMER instruments on the SOHO satellite*", Proc. SPIE* 2518, pp.334-55, 1995.
5. Vallerga, J.; Zaninovich, J.; Welsh, B.; Siegmund, O.; McPhate, J.; Hull, J.; Gaines, G.; Buzasi, D. The FUV detector for the cosmic origins spectrograph on the Hubble Space Telescope, *Nuclear Instruments and Methods in Physics Research Section A*, Volume 477, Issue 1-3, p. 551-555, 2002.
6. O.H.W. Siegmund, J. McPhate, A. Tremsin, J.V. Vallerga, B.Y. Welsh and J.M. Wheatley, *AIP Conference Proceedings*, 984, 103, 2008.
7. O. Siegmund, J. Vallerga, P. Jelinsky, M. Redfern, X. Michalet, S. Weiss, "Cross Delay Line Detectors for High Time Resolution Astronomical Polarimetry and Biological Fluorescence Imaging", *IEEE* 2005 Nuclear Science Symposium and Medical Imaging Conference, Puerto Rico, October 2005.
8. W. Priedhorsky and J. Bloch, *Applied Optics*, 44(3), 423-433, 2004.
9. Michalet, X.; Siegmund, O. H. W.; Vallerga, J. V.; Jelinsky, P.; Millaud, J. E.; Weiss, S., Photon-counting H33D detector for biological fluorescence imaging, *Nuclear Instruments and Methods, Section A*, Vol. 567, Issue 1, p. 133-136. 2006
10. A.S. Tremsin, G.V. Lebedev, O.H.W. Siegmund, et al, High spatial and temporal resolution photon/electron counting detector for synchrotron radiation research, *Nucl. Instrum. and Meth. A*, 580, 853-857, 2006.
11. D. C. Martin, J. Fanson, D. Schiminovich, et al., "The Galaxy Evolution Explorer: A space ultraviolet survey mission", *Astrophysical Journal* **619**, pp. L1-L6, 2005
12. P. Jelinsky, P. Morrissey, James Malloy, S. Jelinsky, and O. Siegmund, C. Martin, D. Schiminovich, K. Forster, T. Wyder & P. Friedman, "Performance Results of the GALEX XDL detectors", *Proc. SPIE*, **4854**, p.233-240, 2002.
13. O.H.W. Siegmund J.V. Vallerga, A. Martin, B. Feller, M. Arif. D. Hussey, and D. Jacobsen, A high spatial resolution event counting neutron detector using microchannel plates and cross delay line readout, *Nucl. Instr. & Meth. A*, 579, 188-191, 2006
14. A. S. Tremsin, O. H. W. Siegmund, J. V. Vallerga, J. Hull, *IEEE Trans. Nucl. Sci.* **51**, pp.1707-1711, 2004

15. O.H.W. Siegmund, A. Tremsin, J.V. Vallerga, J. McPhate, “microchannel plate cross strip detectors with high spatial and temporal resolution”, Nuclear Instruments and Methods, in press 2009
16. Motch, C. et al., 1985, ‘An IR, optical and X-ray study of the two state behaviour of GX 339-4’, *Sp.Sci. Rev*.,40,219
17. Malzac, J. et al., 2004, ‘Jet-disc coupling through a common energy reservoir in the black hole XTE J1118+480’, *MNRAS*, 351, 253
18. Motch, C. et al., 1983, `Simultaneous X-ray/optical observations of GX339-4 during the May 1981 optically bright state’, *A & A*, 119,171
19. Gandhi, P. et al., 2008, ’Rapid optical & V-ray timing observations of GX 339-4’, *MNRAS*, 390, L29
20. Pandel, D. and Cordova, F., 2002, ‘XMM–Newton observes flaring in the polar UZ For during a low state’, *MNRAS*, 336, 1049
21. Bailey, J. and Cropper, M., 1991, ‘The eclipse light curves of UZ For’, *MNRAS*, 253, 27
22. Mauche, C., 2002, ` Correlation of the Quasi-Periodic Oscillation Frequencies of White Dwarf, Neutron Star, and Black Hole Binaries’, *ApJ*, 580, 423
23. Fuhrmeister, B. et al., 2008, ‘Multiwavelength observations of a giant flare on CN Leo’, *A & A*, 487, 293
24. Cargill, P. and Klimchuk, J., 2004, ` Nanoflare Heating of the Corona Revisited’, *ApJ*, 605, 911
25. Ramsay, G. et al., 2004, ‘XMM–Newton observations of polars in low accretion states’, *MNRAS*, 350, 1373
26. Cieslinski, D. and Steiner, J., ‘The orbital period of RX J1141.3-6410’, *MNRAS*, 291, 321
27. Bhat, N. et al., 2008, ‘Bright giant pulses from the Crab Nebula’, *ApJ*, 676, 1200
28. Knight, H. et al., 2005, ‘A search for giant pulses from millisecond pulsars.’, *ApJ*, 625, 951
29. Shearer, A. et al. (2003), ‘Enhanced optical emission during Crab giant radio pulses’, *Science*, 301, 493
30. Middleditch, J. et al. 1987, “Optical color and timing measurements of the 50ms LMC pulsar PSR 0540-69”, *ApJ*, 315, 142